

IAC-13-A6.7.2

ASSESSMENT OF POSSIBLE OBSERVATION STRATEGY IN LEO REGIME

**A. Vananti**

Astronomical Institute University of Bern (AIUB), Bern, Switzerland, [alessandro.vananti@aiub.unibe.ch](mailto:alessandro.vananti@aiub.unibe.ch)

**T. Schildknecht**

Astronomical Institute University of Bern (AIUB), Bern, Switzerland, [thomas.schildknecht@aiub.unibe.ch](mailto:thomas.schildknecht@aiub.unibe.ch)

**G.M. Pinna**

European Space Astronomy Centre (ESAC), Madrid, Spain, [gianmaria.pinna@esa.int](mailto:gianmaria.pinna@esa.int)

**T. Flohrer**

European Space Operations Centre (ESOC), Darmstadt, Germany, [tim.flohrer@esa.int](mailto:tim.flohrer@esa.int)

ABSTRACT

The European Space Agency (ESA) is developing an independent system for Space Situational Awareness (SSA). One component of the draft architecture of the system foresees a network of optical telescopes for observations in the GEO/MEO/LEO regions. The telescope network will survey and track objects up to a certain limiting magnitude and will allow the collection of accurate orbits. Major design drivers are the requirements on coverage of the existing object population, timeliness for detecting particular events, such as, e.g., fragmentations, releases, or orbit maneuvers, and orbit accuracy for cataloguing. In this work, a possible strategy for covering the upper LEO regime by optical observations is analyzed. The visibility limitations of LEO objects observed from stations at different latitudes are evaluated. Coverage simulations of the existing LEO population are performed considering different numbers of sites. Using simulated LEO observations of selected test objects, the orbit determination accuracy depending on different observation intervals is examined.

INTRODUCTION

In the architecture of the future European Space Situational Awareness (SSA) system a network of optical telescopes for observations in Geostationary Earth Orbit (GEO), Medium Earth Orbit (MEO) and Low Earth Orbit (LEO) regions is planned. The telescope network will survey and track space objects to determine accurate orbital data. Several ESA studies were dedicated to observations in GEO [RD-1][RD-2] and MEO [RD-5][RD-6] orbit regions. For the latter possible solutions within an SSA network have been proposed [RD-3][RD-4]. Relatively less research was performed on optical observations in LEO regime. Traditionally, two type of technologies, optical sensors and radars, have been deployed for surveillance of distinct orbital regimes: radars for LEO, optics for the higher Earth orbits. Optical sensors have been redirected to the surveillance of the higher Earth orbits because coverage at long range is a very inefficient process for radars. Optical sensors, taking advantage of the Sun's illumination of targets and being able to have very large fields of view, excel at long range surveillance. From ESA's perspective, cost is a concern in the procurement of a space surveillance radar and it has given rise to the question of how much of the LEO population surveillance could be covered by modern optical sensors. Today, advances in computing and detector

technology have made possible optical sensors with large fields of view and so it is appropriate that the use of optical sensors for the surveillance of LEO should be reexamined. In two distinct ESA studies the issues which need to be addressed, when optical sensors are used for LEO surveillance, were considered and LEO optical sensor system architectures were proposed. One of the developed observation concepts is briefly described in [RD-7]. The strategy uses wide-field telescope with so-called dynamic horizontal fences. The low altitude of the LEO orbits makes it very difficult to find optimal observation geometries and low phase angles are obtained for objects in proximity of the Earth shadow border. The concept of dynamical fence bases on the fact that the position of the fence is changed during the night according to the motion of the shadow border to optimize the phase angle of the acquired observations. The fields are adapted not only during one night but also depending on the day of the year and the position of the station.

In this work, starting from the above-mentioned concept, a possible strategy for covering the upper LEO regime by optical observations is analyzed. In general the performance of the surveillance strategy is evaluated according to three principal requirements: coverage, timeliness, orbit determination accuracy. The coverage refers to the amount of observed objects w.r.t. an existing population. Timeliness is referred to the

detection of particular events, such as, e.g., fragmentations, releases, or orbit maneuvers. Lastly the quality of the catalogued data is given by the accuracy of the determined orbits. In the following we focus on coverage and orbit accuracy. The visibility limitations of LEO objects observed from stations at different latitudes are evaluated. The coverage is addressed with simulations of the existing LEO population considering different numbers of sites. Using simulated LEO observations of selected test objects, the orbit determination accuracy depending on different observation intervals is examined.

**VISIBILITY OF LEO OBJECTS**

At first the visibility of LEO objects from a given site was investigated. One of the limiting factors is the minimal elevation that can be achieved to observe the object. Following the approach with a dynamic fence, observing fields close to the Earth shadow border, the minimal elevation is calculated. In this analysis the following definitions are used. Figure 1 shows the Earth shadow (black circle) and a portion of a possible observation stripe schematically indicated in black around it. The stripe follows first the contour of the shadow (curved part) and then continues parallel to the  $\beta$  axis (straight part). The position of the latter stripe is defined with the angle  $\delta$ . The geocentric shadow diameter for objects at 1000 km altitude is about  $120^\circ$ . The O point is the sun opposition and the location of the observing site is given by  $\theta$  (local time in deg) and  $\lambda$  (latitude). The angles  $\phi$  and  $\beta$  describe the position of the observed field on the curved and straight stripe, respectively. The region of the Earth shadow w.r.t. the equatorial plane is described by  $\varepsilon$ . In summer and winter  $\varepsilon$  varies towards  $\pm 23^\circ$ . Table 1 summarizes the symbols used in the simulations.

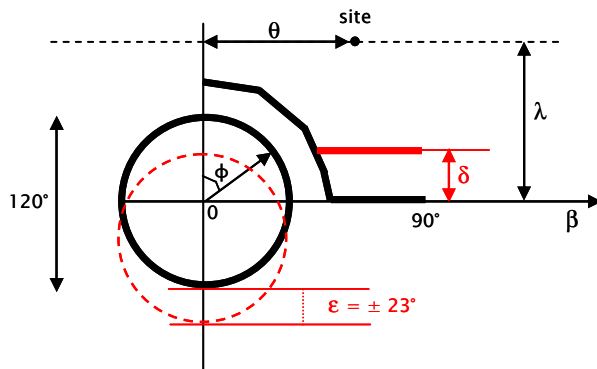


Figure 1. Scheme showing the Earth shadow region (circle) and the observation stripe around it.

Symbol	Description
O	Sun opposition direction projected onto the equatorial plane.
$\theta$	Angular distance between the hour circle through O and the meridian through the observing site.
$\lambda$	Latitude of the observing site.
$\varepsilon$	Angle between Sun opposition direction and O direction.
$\Phi$	Angle describing the position of the observed field (curved part, along the shadow border) starting from the field on the hour circle through O ( $\Phi = 0$ ).
$\delta$	Declination of the observed field (straight part, fixed declination stripe).
$\beta$	Right ascension difference between observed field and O.
Alt	Elevation angle of observed field in the horizontal system.

Table 1. Description of symbols used in the simulations.

The results of the calculations are shown in diagrams as in Figure 2. Here the elevation angles as a function of site position  $\theta$  during the night and observed field  $\phi$  (curved stripe) for  $\lambda=30^\circ$  and  $\varepsilon=0^\circ$  are exhibited. The color legend indicates the elevation angle (or Altitude angle). The shaded areas indicate two moments during the night where the range of visible fields is small ( $\sim 20^\circ$ ) and large ( $\sim 60^\circ$ ). The minimal elevation usually considered for observations is around  $10^\circ$ . Figure 3 exhibits the elevation angles for the straight stripe. The dark shaded area is not to be considered since the straight stripe starts only at  $\beta=60^\circ$ . From the diagram it is evident that for  $\delta=0^\circ$  the objects are never visible because the elevation angles are always below  $0^\circ$ .

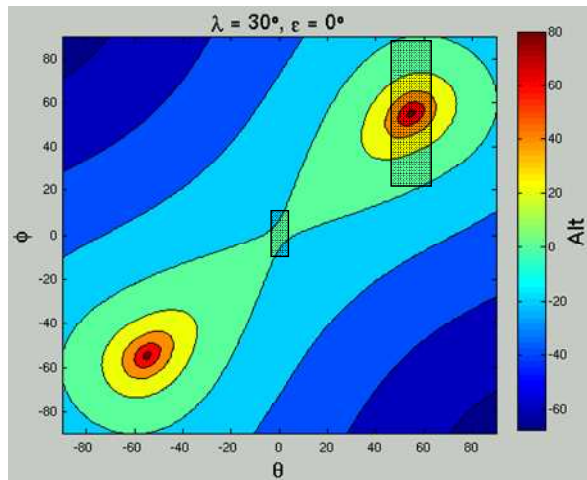


Figure 2. Elevation angles for  $\lambda=30^\circ$  and  $\epsilon=0^\circ$  for curved stripe.

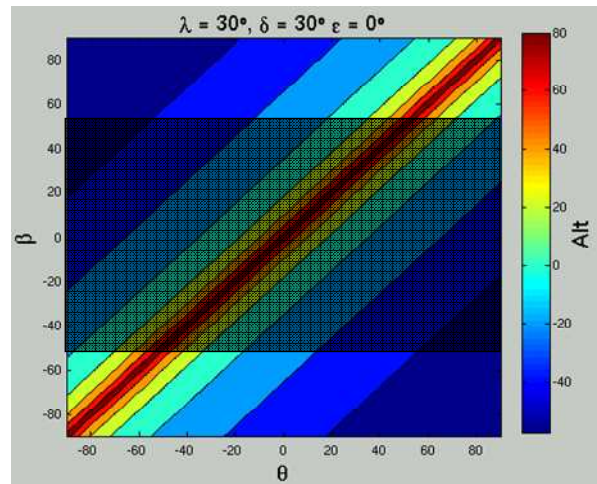


Figure 4. Elevation angles for  $\lambda=30^\circ$ ,  $\delta=30^\circ$ , and  $\epsilon=0^\circ$  for straight stripe.

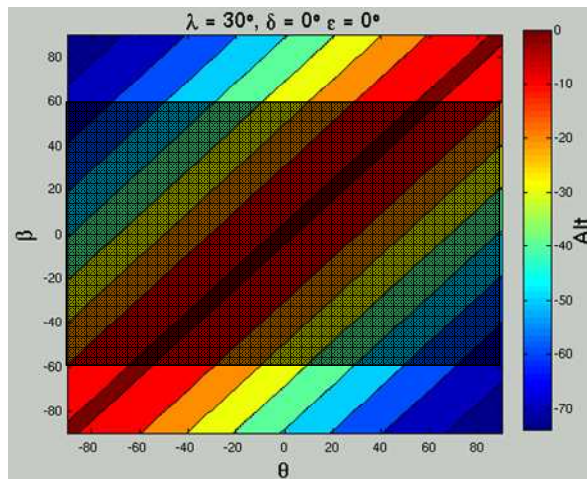


Figure 3. Elevation angles for  $\lambda=30^\circ$ ,  $\delta=0^\circ$ , and  $\epsilon=0^\circ$  for straight stripe.

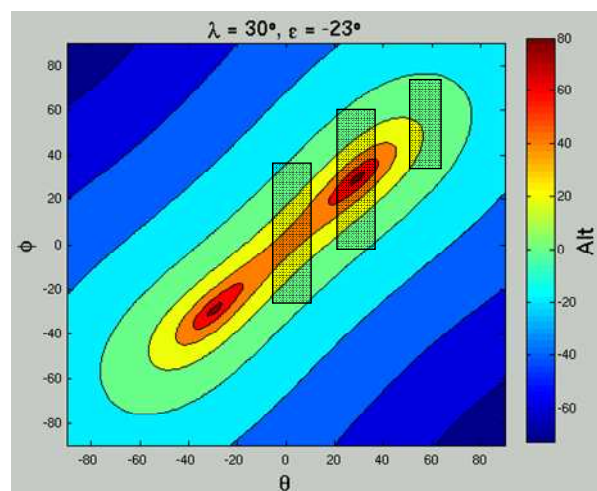


Figure 5. Elevation angles for  $\lambda=30^\circ$  and  $\epsilon=-23^\circ$  for curved stripe.

In Figure 4 a straight stripe at  $\delta=30^\circ$  is assumed and the visibility is very much improved. The drawback of a stripe at higher  $\delta$  is the missing coverage of objects with low inclination. In summer the visibility is better for the period around midnight as shown in Figure 5. Unfortunately in winter the fields of the curved stripe are not visible. Only from sites with  $\lambda=50^\circ$  and higher the objects start to be visible during the whole night. From Figure 4 and Figure 5 it can be seen that the coverage can be imagined like a sliding window that covers around 20°-30° or 1.5-2 hours of the moving site.

Similar to the diagrams for the elevation, the next figures show the phase angles as a function of site position and observed fields using the same above notation. Figure 6 and Figure 7 show the phase angles for the curved stripe in spring/autumn and summer, respectively. The reddish region around midnight exhibits the worst phase angles. In summer the values are slightly better reaching  $90^\circ$ . The shaded regions indicate reasonable angles smaller than  $60^\circ$ . For the straight stripe Figure 8 and Figure 9 evidence the big variation of angles between  $20^\circ$  and over  $100^\circ$ .

In conclusion, the diagrams show that in general the visibility is quite reduced in the curved stripe especially in winter, for stations in the northern hemisphere, and vice versa. For a telescope at  $30^\circ$  latitude in summer the

visibility corresponds to a window along the stripe of about 30°.

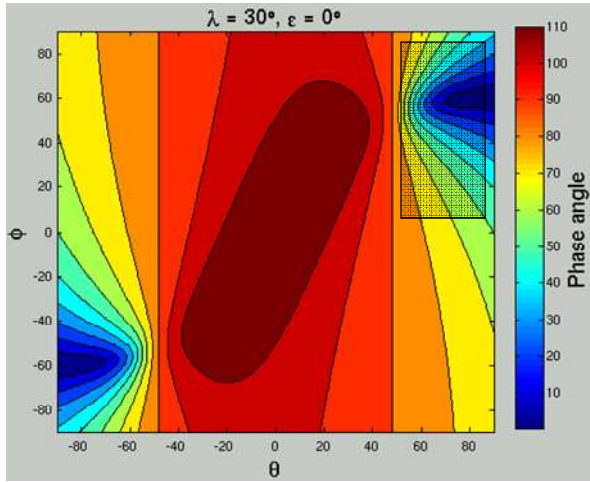


Figure 6. Phase angles for  $\lambda=30^\circ$  and  $\epsilon=0^\circ$  for curved stripe.

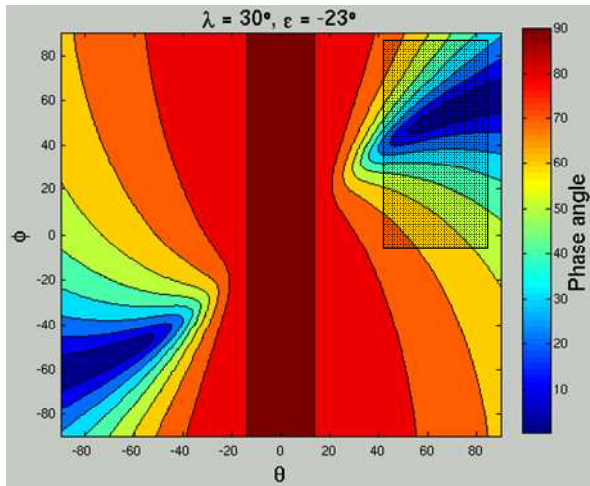


Figure 7. Phase angles for  $\lambda=30^\circ$  and  $\epsilon=-23^\circ$  for curved stripe.

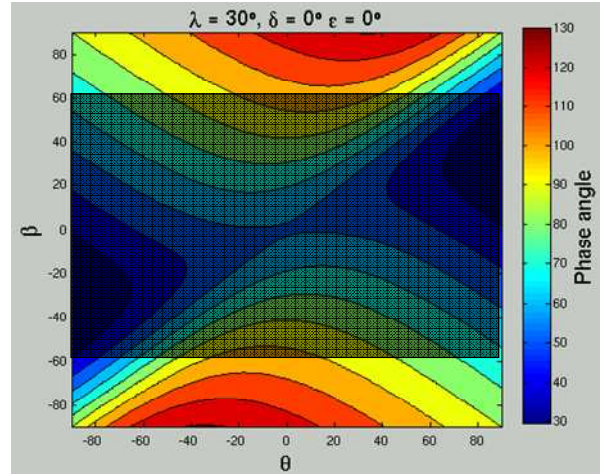


Figure 8. Phase angles for  $\lambda=30^\circ$ ,  $\delta=0^\circ$ , and  $\epsilon=0^\circ$  for straight stripe.

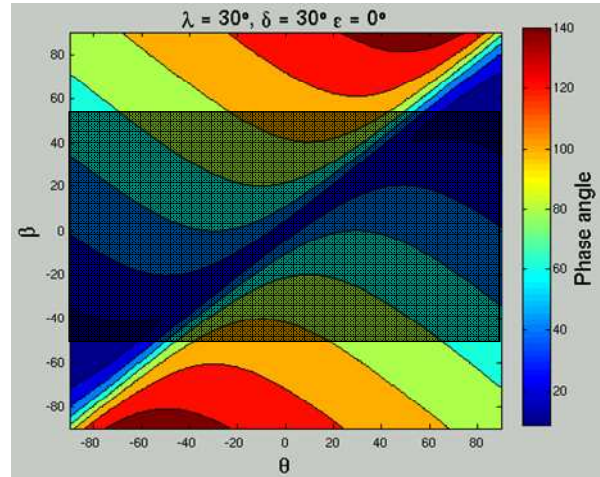


Figure 9. Phase angles for  $\lambda=30^\circ$ ,  $\delta=30^\circ$ , and  $\epsilon=0^\circ$  for straight stripe.

### COVERAGE SIMULATIONS

To investigate the results given in the previous section, coverage simulations have been conducted with the ESA simulation software described in [RD-8]. A TLE population of  $\sim 2000$  objects with eccentricity 0 - 0.05 and inclination  $50^\circ - 100^\circ$  was selected. The altitude of the objects ranges from 1000 km to 2000 km. The observations are performed from 2 different sites, Tenerife and Azores. For the straight stripe a declination  $\delta=30^\circ$  was assumed and for the minimal elevation  $10^\circ$  were considered. Table 2 shows the number of objects visible (illuminated in front of dark background) during one night observing the fields along the curved/straight stripe considered in the visibility diagrams. The maximal coverage is reached observing from 2 stations in summer. However, not all objects can be observed:

most of the missed objects lie in the twilight region and other are only visible below the minimal elevation. In fact simulations from 2 stations in June assuming 0° minimal elevation and neglecting the observation constraints at twilight yield 1953 objects, close to the total population. To ignore the twilight constraints in the simulation the night sky background is set immediately after sunset (sun center at 0° elevation).

	December	June	September
Tenerife	312	989	661
Tenerife + Azores	456	1286	895

Table 2. Number of objects visible observing the fields along the curved/straight stripe.

The coverage at different times during the night is summarized in the following histograms. Figure 10, Figure 11, and Figure 12 illustrate the percentage of visible objects from Tenerife during one night in September, December, and June, respectively. The percentage refers to the entire considered population of around 2000 objects. A gap of about 4 hours around midnight can be noticed. This corresponds to the area of limited visibility also found in Figure 2. The approximate coverage of the sliding window can be roughly read from the gap diagrams and is about 2 hours, or 30°. In winter the nights are longer but the visibility for LEO is even more reduced. In summer, during around 3 months there is no visibility gap around midnight. The only limitation is due to the twilight region. Figure 13 displays the coverage assuming 0° minimal elevation and neglecting twilight constraints: the coverage is extended of about 2 hours.

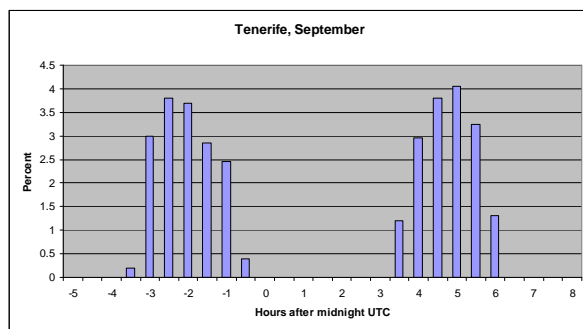


Figure 10. Percentage of visible objects from Tenerife during one night in September.

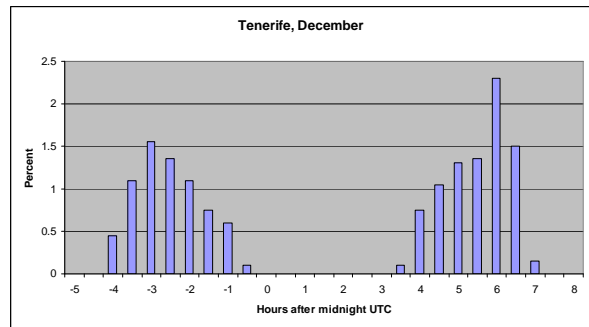


Figure 11. Percentage of visible objects from Tenerife during one night in December.

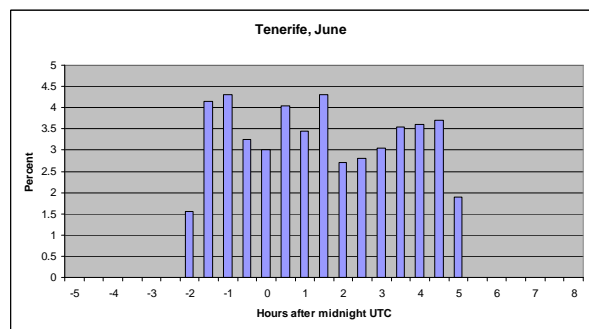


Figure 12. Percentage of visible objects from Tenerife during one night in June.

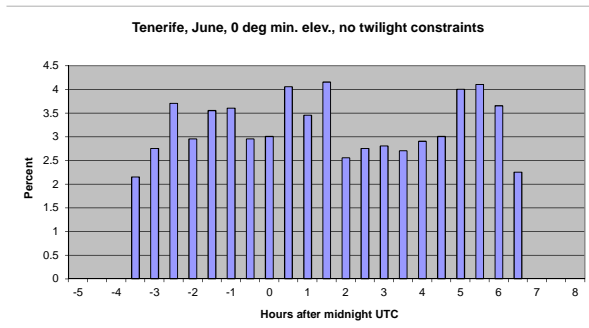


Figure 13. Percentage of visible objects from Tenerife during one night in June assuming 0° minimal elevation and neglecting twilight constraints.

### ORBIT DETERMINATION

In addition to the coverage, the orbit determination accuracy is another key factor that influences the observation strategy. Simulated orbits of 100 LEO objects were used to generate synthetic observations. The orbits determined from these observations were then compared with the original simulated orbits. In the simulated observations a mean astrometric error of 0.5'' was considered. Note that this assumption requires some effort for LEO, as it involves proper streak detection and reduction, or short exposure times, what limits the

number of stars in the FOV. In the simulations the discovery observations of the objects are taken from Tenerife, at midnight UTC of the 21.09.12. Every tracklet consists of 3 subsequent observations within 15 s. The LEO population was selected with altitude range 1000 km - 2000 km, eccentricity 0 - 0.01, and inclination  $60^\circ$  -  $85^\circ$ . The ascending node and the anomaly were restricted in order to have visible objects within a region of about  $5^\circ$  in right ascension and  $30^\circ$  declination around the zenith, observing from Tenerife at the discovery epoch.

The Figure 14 shows the angular position error as a function of the elapsed time. The starting time corresponds to the first observation. After 5 minutes a second series of observations was simulated, which is clearly visible in the diagram with a reduction of the error. The period of 5 minutes corresponds approximately to a second stripe close to the one in which the first tracklet is observed. Figure 15 illustrates the histogram with the percentage of the angular position error after 24 hours. The observations were simulated after 5 minutes and 2 hours. The latter would be approximately one revolution period. The error for the most orbits varies between  $0.1 \cdot 10^{-3}$  deg ( $\sim 0.3''$ ) and  $1.5 \cdot 10^{-3}$  deg ( $\sim 5.5''$ ). The histogram shows a peak around  $0.4 \cdot 10^{-3}$  deg. To improve the accuracy additional simulated observations after 4 hours were included in the orbit determination in Figure 16. The peak in the error in this case is around  $1''$ . Figure 17 exhibits the simulations with observations after 20 minutes and 2 hours. In our hypothetical scenario the second series of observations is taken by another station from which the object is visible after 20 minutes. The location could be e.g. in the southern hemisphere at a longitude similar to the one of the first station. The peak also lies around  $1''$  with a slightly smaller percentage than in the case with observations after 4 hours. In Figure 18 and Figure 19 the almost ideal case with observations after every 2 hours is shown. Over 60% of the orbits are determined with accuracy well below  $1''$ . Note that in this simulations a proper correlation of reobserved objects is assumed, with 100% success rate.

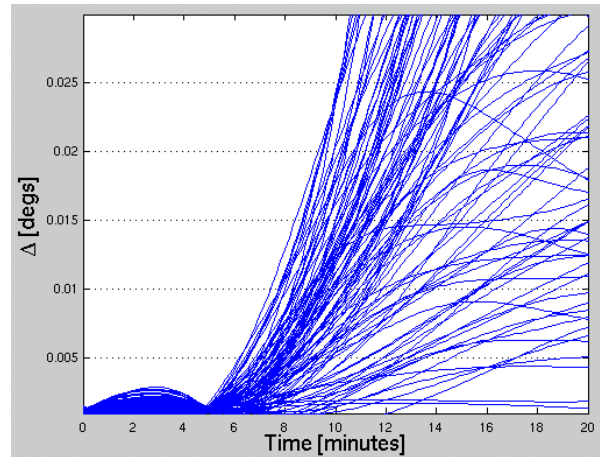


Figure 14. Angular position error vs. elapsed time. Observations after 5 minutes.

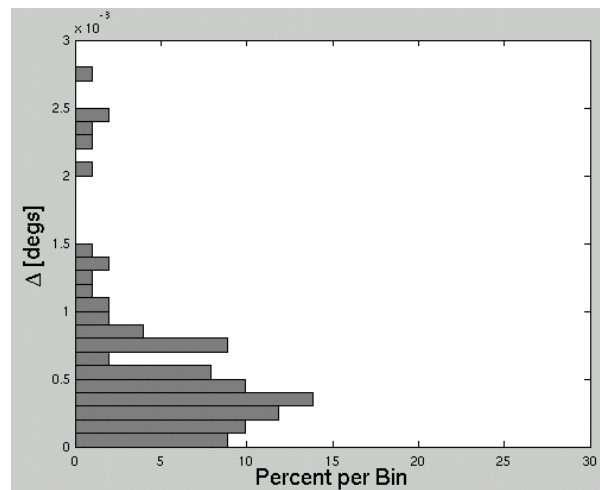


Figure 15. Histogram of the angular position error after 24 hours. Observations after 5 minutes and 2 hours.

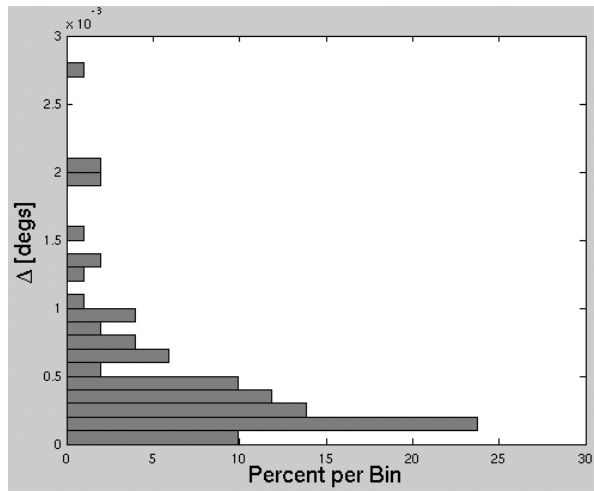


Figure 16. Histogram of the angular position error after 24 hours. Observations after 5 minutes, 2 hours, and 4 hours.

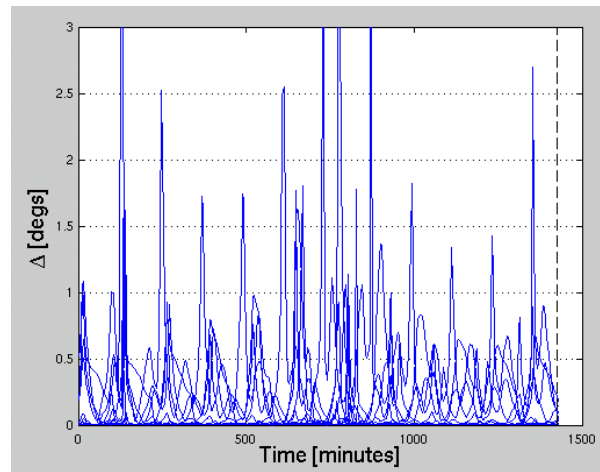


Figure 18. Angular position error vs. elapsed time. Observations after 5 minutes and every 2 hours until 24 hours.

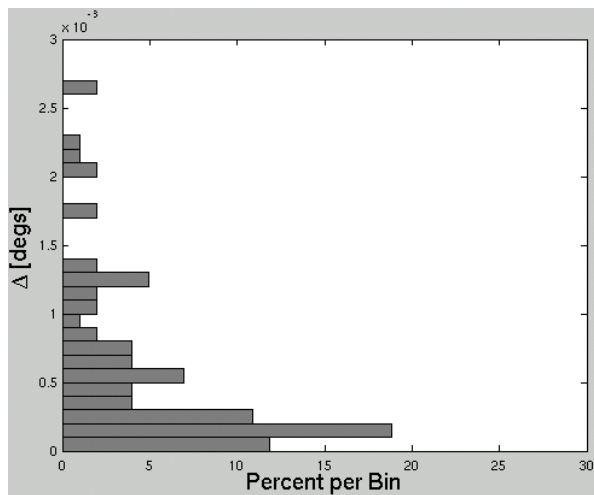


Figure 17. Histogram of the angular position error after 24 hours. Observations after 20 minutes and 2 hours.

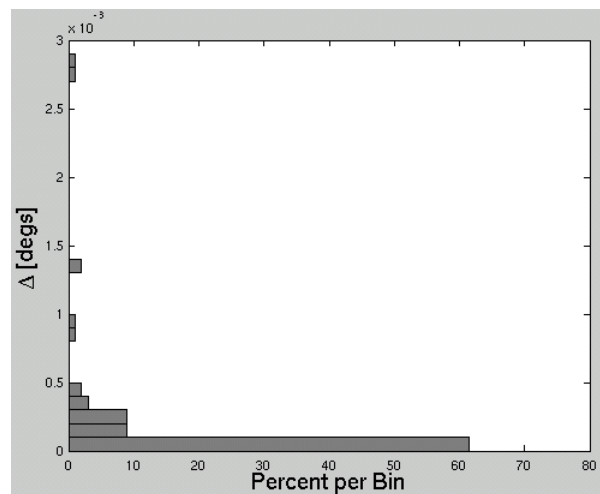


Figure 19. Histogram of the angular position error after 24 hours. Observations after 5 minutes and every 2 hours until 24 hours.

To compare the results with the requirements defined within the SSA framework the output of the simulations was expressed in radial, along-track, and out-of-plane components of the state vector error. Figure 20 illustrates as an example the along-track component of the position error in the scenario with follow-ups after 20 minutes and 2 hours. The corresponding histograms for the radial and along-track component of the position error are shown in Figure 21 and Figure 22. In the following analysis the latter components are considered as representative for the obtained accuracy. We assume 4 m and 30 m for the required radial and along-track accuracy, respectively. The strategy illustrated in Figure 21 and Figure 22

seems to partly satisfy the requirements. Conversely follow-ups after 5 minutes and only after 2 hours are not enough to reasonably satisfy the requirements, as indicated in Figure 23 and Figure 24. In the scenario with follow-ups after 5 minutes, 2 hours, and 4 hours, the histograms in Figure 25 and Figure 26 exhibit an amount around 50% within the requirements for radial and along-track component. Obviously the accuracy is much improved for the ideal scenario with observations every 2 hours as illustrated in Figure 27. For the most critical along-track component the histogram indicates that > 90% of the orbits reside in the required accuracy range.

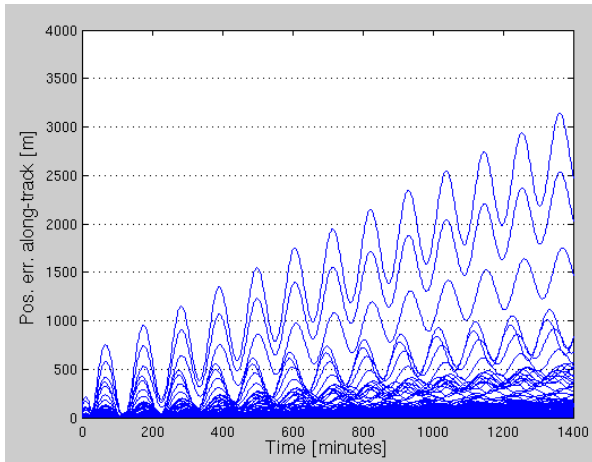


Figure 20. Along-track component of position error vs. elapsed time. Observations after 20 minutes and 2 hours.

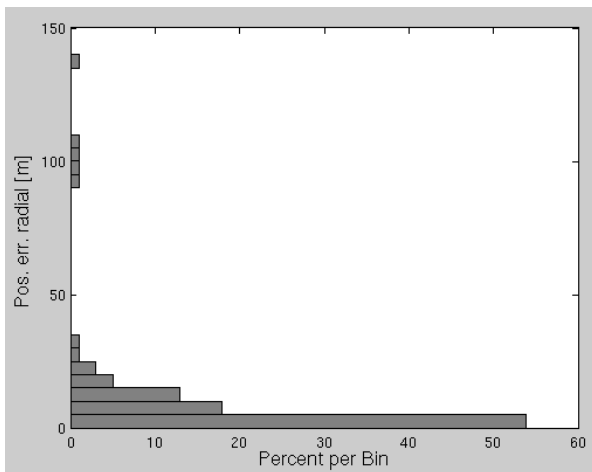


Figure 21. Histogram of radial component of position error after 24 hours. Observations after 20 minutes and 2 hours.

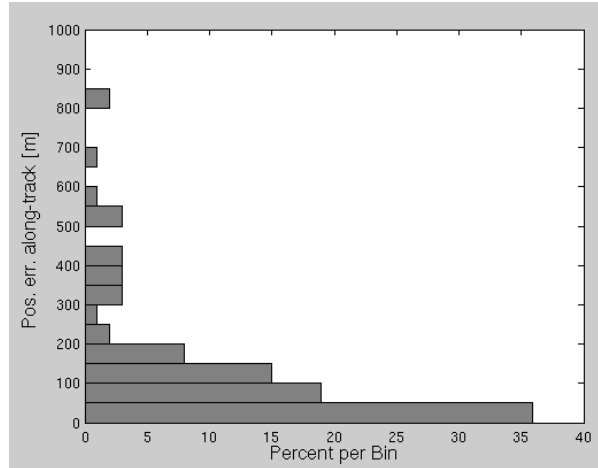


Figure 22. Histogram of along-track component of position error after 24 hours. Observations after 20 minutes and 2 hours.

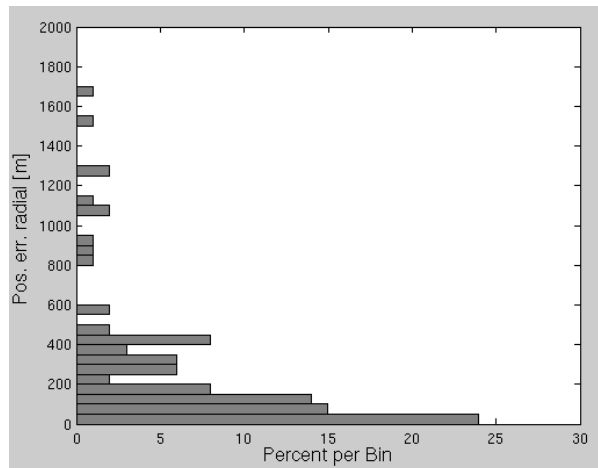


Figure 23. Histogram of radial component of position error after 24 hours. Observations after 5 minutes and 2 hours.

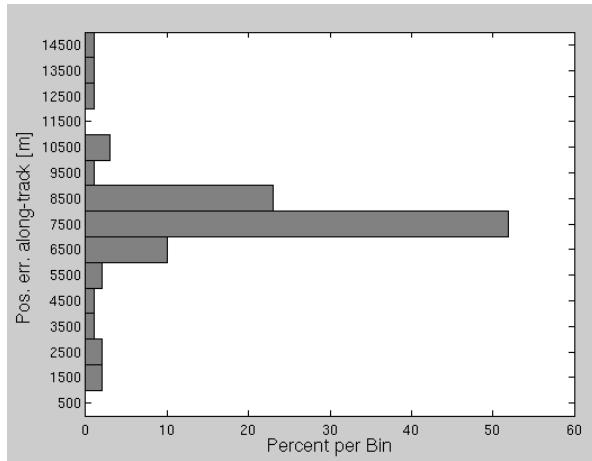


Figure 24. Histogram of along-track component of position error after 24 hours. Observations after 5 minutes and 2 hours.

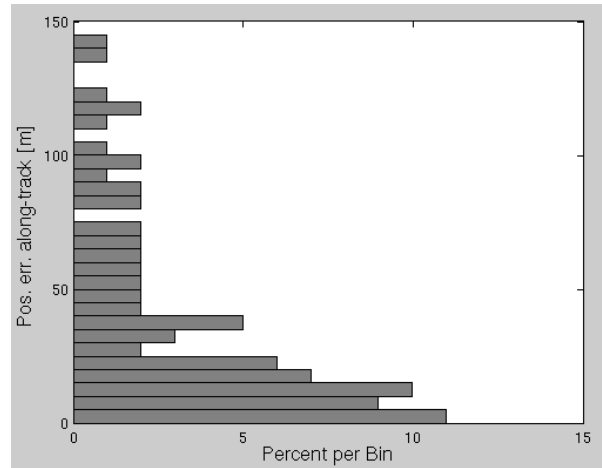


Figure 26. Histogram of along-track component of position error after 24 hours. Observations after 5 minutes, 2 hours, and 4 hours.

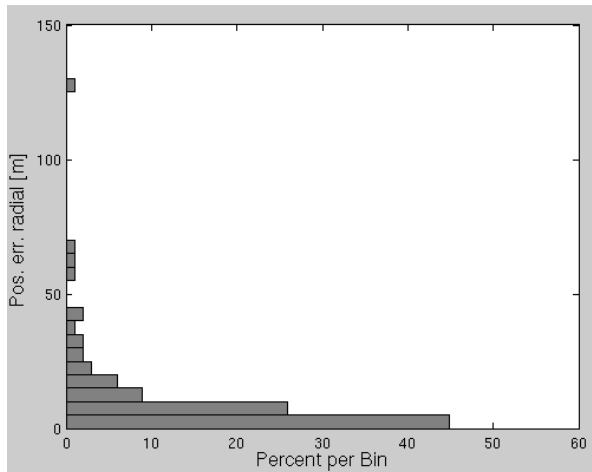


Figure 25. Histogram of radial component of position error after 24 hours. Observations after 5 minutes, 2 hours, and 4 hours.

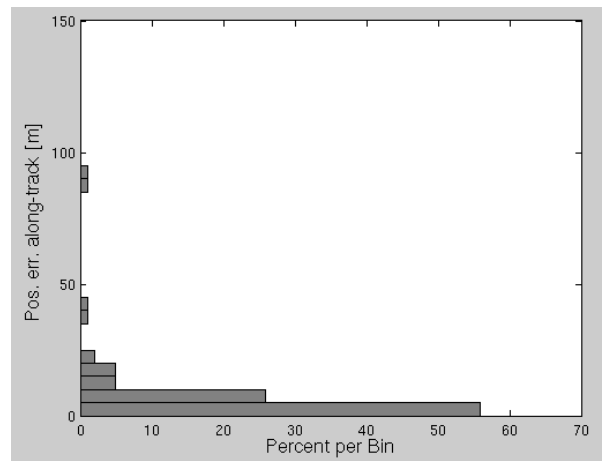


Figure 27. Histogram of along-track component of position error after 24 hours. Observations after 5 minutes and every 2 hours until 24 hours.

### CONCLUSIONS

The visibility limitations for LEO objects are determined by the minimal elevation that can be reached during astronomical observations, in general  $\sim 10^\circ$ . The ideal strategy needs an observation stripe which follows the contour of the Earth shadow and continues with approximately constant declination. Diagrams for a telescope at  $30^\circ$  latitude, depending on time of the night, observed fields, and period of the year, show that the visibility is in general reduced to a window along the stripe of about  $30^\circ$ . Also, for most of the year, except in summer, during about 4 hours of the night, the stripe can not be observed. Sites at high latitude would be of advantage, but not indispensable, in order to fill the visibility gap. The phase angles remain mostly around

60° and less, but there are few situations with more than 90°.

Observation simulations from Tenerife and Azores of a LEO TLE population (1000-2000 km altitude) confirm the results indicated by the diagrams. About 65% of the population can be observed in summer and 25% in winter. In addition to the minimal elevation, one of the limiting factors is the twilight (20% reduction).

The orbit determination from simulated LEO observations with 0.5'' error, without considering drag, and assuming 100% correlation success of observations, indicates that a two stripes strategy is needed to reach reasonable accuracies after 24 hours. Nevertheless this degree of accuracy is reached only for part of the object population. Two situations were analyzed:

- 1 site in the northern and 1 site in the southern hemisphere at similar longitudes. Follow-ups after 20 minutes and 2 hours.
- 2 sites in same hemisphere with about 30° separation in longitude. Follow-ups after 5 minutes, 2 hours, and 4 hours.

In both situations on average more than 50% of the orbits meet the assumed accuracy requirements. Further improvement can be obtained with even more sites distributed in longitude.

#### ACKNOWLEDGEMENTS

This work was done under ESA contract 4000105867/12/D/MRP.

#### REFERENCES

- [RD-1] Schildknecht, T., R. Musci, M. Ploner, G. Beutler, W. Flury, J. Kuusela, J. de Leon Cruz, L. de Fatima Dominguez Palmero, Optical observations of space debris in GEO and in highly-eccentric orbits, *Advances in Space Research*, 34, 2004
- [RD-2] Schildknecht, T., T. Flohrer, R. Musci, R. Jehn, Statistical analysis of the ESA optical space debris surveys, *Acta Astronautica*, 63, 2008
- [RD-3] Flohrer, T., T. Schildknecht, R. Musci, E. Stöveken, Performance estimation for GEO space surveillance, *Advances in Space Research*, 35, 2005
- [RD-4] Flohrer, T., T. Schildknecht, R. Musci, Proposed strategies for optical observations in a future European Space Surveillance network, *Advances in Space Research*, 41, 2008
- [RD-5] Hinze, A., T. Schildknecht, A. Vananti, H. Krag, Results from first space debris survey observations in MEO, *Proceedings of European Space Surveillance Conference*, Madrid, Spain, 2011
- [RD-6] Hinze, A., T. Schildknecht, T. Flohrer, H. Krag, Results of space debris survey observations on highly-eccentric MEO orbits, *Proceedings of 6th European Conference on Space Debris*, Darmstadt, Germany, 2013
- [RD-7] Cibirin, L., M. Chiarini, A. Bertoli, F. Villa, L. Dimare, D. Farnocchia, F. Bernardi, A. Milani, G.M. Pinna, I. Zayer, P.M. Besso, R. Ragazzoni, A. Rossi, A dynamic observation concept as a key point for an enhanced SSA optical network, *Proceedings of European Space Surveillance Conference*, Madrid, Spain, 2011
- [RD-8] Munoz, P., J. Fernandez, A. Cendrero, A. Agueda, CO-V Telescope Analysis and Design – Scheduling Simulator Software User Manual, *ESA report*, GMV, Madrid, Spain, 2011